Statistical geometry of cavities in a metastable confined fluid

Aleksey Vishnyakov,[1] Pablo G. Debenedetti,[2] and Alexander V. Neimark[1,*]
[1]*TRI/Princeton, 601 Prospect Avenue, Princeton, New Jersey 08540*
[2]*Chemical Engineering Department, Princeton University, Princeton, New Jersey 08544*
(Received 24 January 2000)

The statistical geometry of cavities in a confined Lennard-Jones (LJ) fluid is investigated with the focus on metastable states in the vicinity of the stability limit of the liquidlike state. For a given configuration of molecules, a cavity is defined as a connected region where there is sufficient space to accommodate an additional molecule. By means of grand canonical Monte Carlo simulations, we generated a series of equilibrium stable and metastable states along the adsorption-desorption isotherm of the LJ fluid in a slit-shaped pore of ten molecular diameters in width. The geometrical parameters of the cavity distributions were studied by Voronoi-Delaunay tessellation. We show that the cavity size distribution in liquidlike states, characterized by different densities, can be approximated by a universal log-normal distribution function. The mean void volume increases as the chemical potential μ and, correspondingly, the density decreases. The surface-to-volume relation for individual cavities fulfills the three-dimensional scaling $S_{\mathrm{cav}}=gV_{\mathrm{cav}}^{2/3}$ with the cavity shape factor $g=8.32-9.55$. The self-similarity of cavities is observed over six orders of magnitude of the cavity volumes. In the very vicinity of the stability limit, $\mu\rightarrow\mu_{sl}$, large cavities are formed. These large cavities are ramified with a fractal-like surface-to-volume relation, $S_{\mathrm{cav}}\propto V_{\mathrm{cav}}$. Better statistics are needed to check if these ramified cavities are similar to fragments of a spanning percolation cluster. At the limit of stability, the cavity volume fluctuations are found to diverge as $(\langle V_{\mathrm{cav}}^2\rangle-\langle V_{\mathrm{cav}}\rangle^2)\propto[(\mu-\mu_{\mathrm{sl}})/kT]^{-\gamma_c}$ with the exponent $\gamma_c\approx 0.93$. This exponent can be referred to as the cavity pseudocritical exponent, in analogy with the other pseudocritical exponents characterizing the divergence of thermodynamic quantities at the spinodal point.

PACS number(s): 61.20.Gy, 68.45.Da, 64.75.+g, 64.70.Fx

I. INTRODUCTION

The formation of metastable states in fluids confined in narrow pores and associated spinodal transitions are well established both experimentally and theoretically [1–3]. In particular, at subcritical conditions the pressures corresponding to the vapor-liquid (capillary condensation) and liquid-vapor (capillary evaporation) transitions in a porous medium may differ, resulting in adsorption hysteresis. Reproducible hysteresis is well documented for adsorption and desorption isothermal cycles for a number of adsorbates on different natural minerals, soil particles, and synthetic adsorbents, including well characterized porous glasses and mesoporous molecular sieves [1–5]. The hysteresis phenomenon is described by different theoretical models of adsorption, including density functional theory, molecular dynamics, and Monte Carlo (MC) simulations (e.g., [4–15]). However, no theoretical method is able to predict quantitatively the inner and upper boundaries of the hysteresis regime, which are related to the experimental stability limits of the corresponding metastable states. The most advanced canonical ensemble density functional theory of adsorption hysteresis [16] and matched MC simulations [17] agree well with experimental observations on mesoporous molecular sieves with pores wider than 5 nm and overestimate the width of the hysteresis loop in narrower pores. Such discrepancies may originate in the molecular mechanisms of cavitation in narrow pores and formation of nuclei, which are poorly understood.

In this paper, we study the statistical geometry of intermolecular cavities in a confined Lennard-Jones (LJ) fluid with the focus on metastable states in the vicinity of the stability limit of the liquidlike state. This approach was quite successful in studies of metastability and phase transitions in the bulk, since valuable insight into the thermodynamic properties of model fluids was gained from studying the statistical geometry of cavity distributions [18–20]. In particular, for the hard sphere fluid [18,19] the thermodynamics can be expressed entirely in terms of these geometrical quantities. For a given configuration of N molecules in volume V, a cavity is defined as a connected region where there is sufficient space to accommodate an additional molecule. The idea of using intermolecular voids for thermodynamic analyses dates back to Boltzmann [21], who calculated the second virial coefficient of the hard sphere gas from the surface-to-volume ratio of the void space. Speedy [18] discussed the geometry and thermodynamics of a hard sphere fluid in terms of exclusion volumes that lie within one diameter of a certain number of spheres. He derived an equation of state for the hard sphere fluid written in terms of the volume and surface area of the void space in the system. Speedy and Reiss theoretically predicted the number and size of cavities in two- and three-dimensional hard sphere systems [19]. Their estimates agree well with the results of molecular dynamics simulation of a two-dimensional hard disk fluid [22]. However, the authors concluded that their theoretical estimates were not accurate enough to reproduce the equation of state or to improve the understanding of the freezing transition. A superheated bulk LJ liquid with constrains imposed to prevent cavitation was studied by Corti and Debenedetti [20,23]. The authors introduced a void constraint ensemble,

*Author to whom correspondence should be addressed. Electronic address: aneimark@triprinceton.org

where limits were imposed on the maximum size of cavities that were allowed to form. A statistical analysis of the void volume distribution was performed to determine when the constrains led to unphysical results. It was found that there is a limit beyond which the constraints, if artificially severe, may have a significant effect on the equation of state.

We show that the geometrical analysis of molecular configurations in terms of intermolecular cavities can shed light on the evolution of metastable states in a confined fluid approaching the stability limit and also on the so-called pseudocritical behavior of a confined fluid at the spinodal point. Although the pseudocriticality at the spinodal of the bulk liquid-gas diagram has been considered earlier in detail (e.g., [24–26]), no attempts have been made to apply this concept to spontaneous capillary condensation and desorption transitions in mesopores.

We study metastable states and the associated spinodal transitions for the condensation-desorption hysteresis cycle of a LJ fluid in a slit-shaped pore of ten molecular diameters in width. The fluid-fluid and fluid-solid parameters were chosen to model nitrogen sorption in carbon nanopores at the nitrogen boiling temperature of 77 K. Equilibrium states along the adsorption-desorption isotherm are generated using the grand canonical Monte Carlo (GCMC) technique. The statistical properties of cavity size and shape distributions are investigated using the algorithm developed recently by Sastry and co-workers [27–29] for the exact calculation of void connectivity, volume, and surface area in dense sphere packings.

II. SIMULATIONS

A. GCMC simulations of capillary condensation and desorption in a slit-shaped pore

We performed GCMC simulations of adsorption and desorption of the Lennard-Jones fluid in slit-shaped pores. The parameters of fluid-fluid and solid-fluid interactions were chosen to model sorption of nitrogen at its boiling temperature (77.4 K) in carbon nanopores, which is a typical and experimentally well studied system [3]. LJ parameters $\sigma_{ff}=3.6154$ Å and $\epsilon_{ff}/k=101.5$ K were used for nitrogen. The potential was cut off at $5\sigma_{ff}$ and not shifted. These parameters provide the best fit to table data on the vapor-liquid equilibrium of bulk nitrogen, as calculated with the equation of Johnson, Zollweg, and Gubbins [30]. The nitrogen boiling temperature 77.4 K corresponds to $0.762\epsilon_{ff}/k$. The solid-liquid interactions were described by the 10-4-3 adsorption potential of Steele with parameters corresponding to the nitrogen-graphite interaction: $\sigma_{sf}=3.494$ Å, $\epsilon_{sf}/k=53.22$ K, $\Delta=3.4$ Å [31]. The simulations were performed in a pore of 10σ in diameter. The pore width was measured between the centers of the carbon atoms in the outer layer of the graphite wall. The basic simulation cell was square in the plane parallel to the walls and had a size of $10\sigma_{ff}\times 10\sigma_{ff}$. Periodic boundary conditions were imposed.

By varying the chemical potential μ, we traced the equilibrium states along the adsorption-desorption isotherm (Fig. 1). At each chemical potential the fluid was equilibrated for 6×10^6 configurations and then statistics were collected over 9×10^6 configurations. According to the equation of Johnson *et al.* [30], for the LJ fluid with 5σ cutoff, the bulk liquid-vapor coexistence point at the temperature $T=0.762\epsilon/k$ corresponds to the chemical potential $\mu_0=-9.35\epsilon$. At these conditions of bulk saturation, the confined fluid forms nine pronounced dense adsorbed layers (Fig. 2, curve 1).

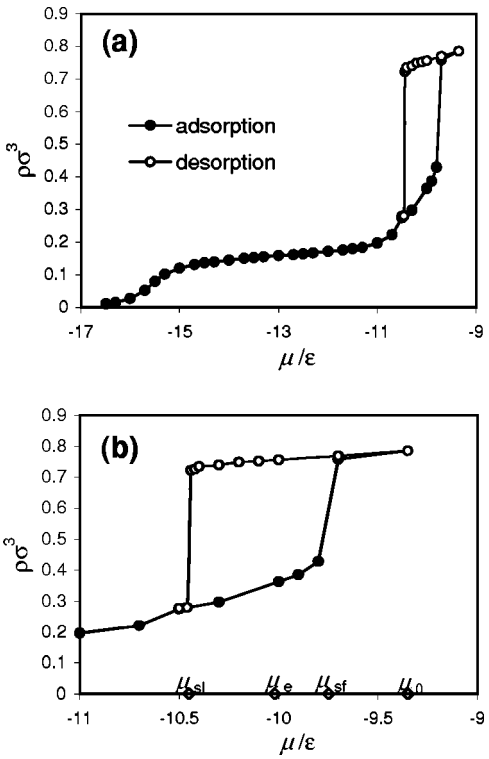

FIG. 1. (a) Adsorption isotherm of Lennard-Jones nitrogen in a carbon slitlike pore of $10\sigma_{ff}$ width at $T=0.762\epsilon/k$; (b) detail of the hysteresis region displaying the location of vapor-liquid equilibrium in the bulk system μ_0 and the pore μ_e, and spontaneous capillary condensation (μ_{sf}) and capillary evaporation (μ_{sl}) transitions.

Reducing the chemical potential, we generated equilibrium liquidlike states along the desorption branch until the system achieved a limit of stability and underwent a spinodal transition associated with the spontaneous desorption (evaporation) of fluid and the formation of an equilibrium adsorption film on the pore walls. The spontaneous desorp-

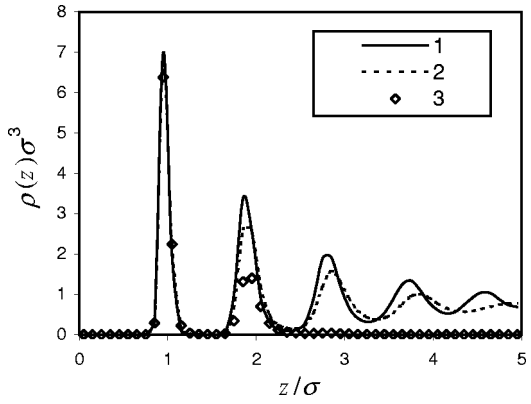

FIG. 2. Density distributions in the condensed fluid: (1) at bulk saturation conditions, $\mu=-9.35\epsilon$; (2) close to the spinodal transition in the metastable liquidlike state on the desorption branch, $\mu=-10.44\epsilon$; (3) in a stable film on the desorption branch, $\mu=-10.5\epsilon$.

tion transition was observed at $\mu_{sl}=-10.44\epsilon$. For $\mu=-10.44\epsilon$, we performed four independent simulation runs starting from different liquid phase configurations. In every one of these simulation runs the system reached an equilibrium liquidlike state, remained in this state for several millions of trial insertions and deletions, and then experienced a rapid transition to a stable filmlike state. The longest simulation of the confined liquid at $\mu=-10.44\epsilon$ consisted of 1.2×10^7 trial insertions. The density profiles for the metastable liquidlike and stable filmlike states at $\mu=-10.44\epsilon$ are presented in Fig. 2, curves 2 and 3, in comparison with the density profile at the saturation conditions, curve 1. Slightly above the estimated spinodal point at $\mu=-10.42\epsilon$, the system remained in a liquidlike state for 9×10^7 simulation steps and showed no tendency to transform into a low density state. Slightly below the estimated spinodal point at $\mu=-10.50\epsilon$, the system transformed sharply (within the first 2×10^6 trial insertions) from the initial liquidlike state to a stable filmlike state, where it remained during additional 9×10^6 simulation steps. Transitions from stable filmlike states to metastable liquidlike states were not observed, as expected.

The adsorption branch was simulated starting from the smallest vapor pressures detectable in the adsorption experiments. These states are presented on an expanded scale in Fig. 1(b). We observed the formation of an adsorbed monolayer at $\mu\approx-(15-11)\epsilon$ and then the growth of a multilayer film. The film configuration became unstable at $\mu_{sf}\approx-9.75\epsilon$, where the system exhibited another spinodal transition associated with the spontaneous condensation and formation of a liquidlike state of capillary condensed fluid.

The point of equilibrium capillary condensation transition has been estimated by the thermodynamic integration method of Peterson and Gubbins [32]. The chemical potential of condensed fluid–adsorbed film–vapor coexistence was estimated as $\mu_e=-10.02\epsilon$, exhibiting a substantial shift from the bulk liquid–vapor coexistence point $\mu_0=-9.35\epsilon$. Thus, the liquidlike states of a condensed fluid along the desorption branch of the isotherm are thermodynamically stable at $\mu_e<\mu<\mu_0$, and metastable at $\mu_{sl}<\mu<\mu_e$ (Fig. 1). Correspondingly, the filmlike states of an adsorbed fluid along the adsorption branch of the isotherm are stable at $\mu<\mu_e$ and metastable at $\mu_e<\mu<\mu_{sf}$. It is worth noting that every one of these states is an equilibrium state.

The observed hysteresis behavior of the capillary condensation-desorption isotherms is typical for most nanoporous materials [3]. For nitrogen sorption at 77.4 K, the capillary condensation hysteresis has been experimentally documented for various materials with pores in the range 4–200 nm [1,3–5], including porous carbon [33,34]. A discussion of the hysteretic nature of capillary condensation phenomena is beyond the scope of this paper. In the following parts we focus on the metastable liquidlike states along the desorption branch of the isotherm, specifically on the evolution of the molecular geometry of a confined liquid in the vicinity of the spinodal transition at $\mu\rightarrow\mu_{sl}$.

B. Statistical geometry of the confined fluid

When considering the microscopic structure of a fluid, we usually deal with descriptions involving the centers of molecules. The mutual distribution of molecules is usually characterized in terms of correlation functions of different order [35]. Additional information on the molecular geometry can be obtained from an analysis of intermolecular cavities [18–23]. We have studied the cavity distribution in liquidlike states along the desorption branch of the capillary condensation isotherm generated by GCMC in the range of chemical potentials from saturation to the spinodal desorption point. To analyze the void geometry in a given configuration obtained by the GCMC simulation, the simulation cell is divided into occupied and void regions. The occupied region is composed of exclusion spheres built around each molecular center. A two-dimensional sketch describing the definition of intermolecular voids is presented in Fig. 3. The radius of the exclusion sphere is chosen from the condition that the probability of insertion of an additional molecule, the center of which lies within the exclusion sphere, is vanishingly small. For the hard sphere fluid, the radius of the exclusion volume equals the molecular diameter. For the LJ fluid, the radius of the exclusion sphere was set equal to σ_{ff}. The void region is composed of disconnected cavities. By definition, two points belong to the same cavity if there exists a continuous path in the void region connecting these points. In Fig. 4 we present a snapshot of a typical cavity observed in our simulations. The cavities have an irregular shape and are characterized by

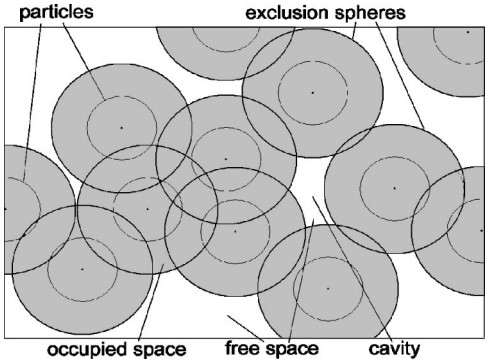

FIG. 3. Two-dimensional sketch showing occupied space (in gray) and void region (in white) composed of disconnected cavities.

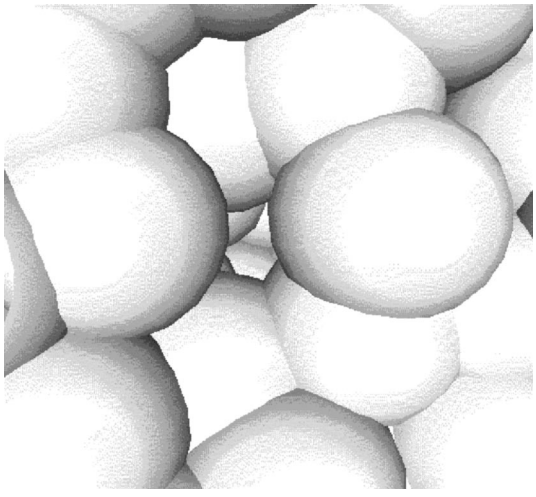

FIG. 4. Snapshot of a cavity in the confined fluid. Gray spheres show exclusion spheres.

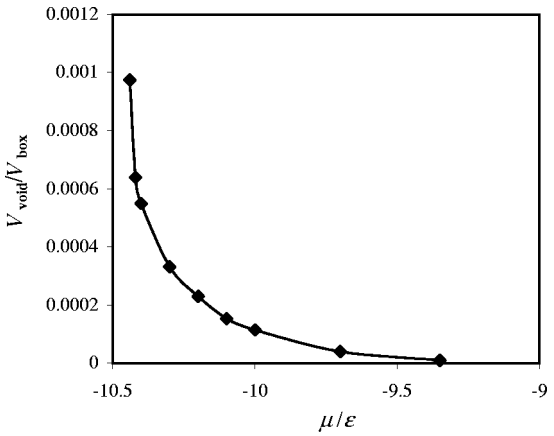

FIG. 5. Dependence of the total void volume in the system, related to the volume of the simulation box, on the chemical potential of the fluid.

their volume and surface area. As the fluid density decreases, the void density and accordingly the number and dimensions of cavities increase.

The cavity analysis was performed by a technique recently introduced by Sastry *et al.* [27] to study dense sphere packings. The method, which allows the exact calculation of void connectivity and cavity volume and surface distributions, is based on the Voronoi-Delaunay tessellation applied to the configuration of molecular centers generated by the GCMC simulation. The tessellation was performed using the algorithm of Tanemura, Ogawa, and Ogita [36]. This technique was designed for systems periodic in all three dimensions. The confined system under consideration here is finite in the direction normal to the pore walls. In order to apply the algorithm to the confined fluid, a close-packed layer of ghost fluid molecules located on the same plane as the outer layer of solid molecules was added to the system. The addition of this layer prevents finding unphysical cavities ''penetrating'' the pore walls. Since in both liquidlike and film states the first layer of adsorbed molecules has the density of a packed monolayer (see Fig. 2), the introduction of the layer of dummy molecules does not influence configurations of the actual intermolecular cavities in the fluid. Because the Voronoi-Delaunay tessellation is computationally intensive, the cavity analysis was performed for molecular configurations obtained every 10^4 GCMC steps. Thus, statistics on the cavities was collected over 900 configurations for each state point.

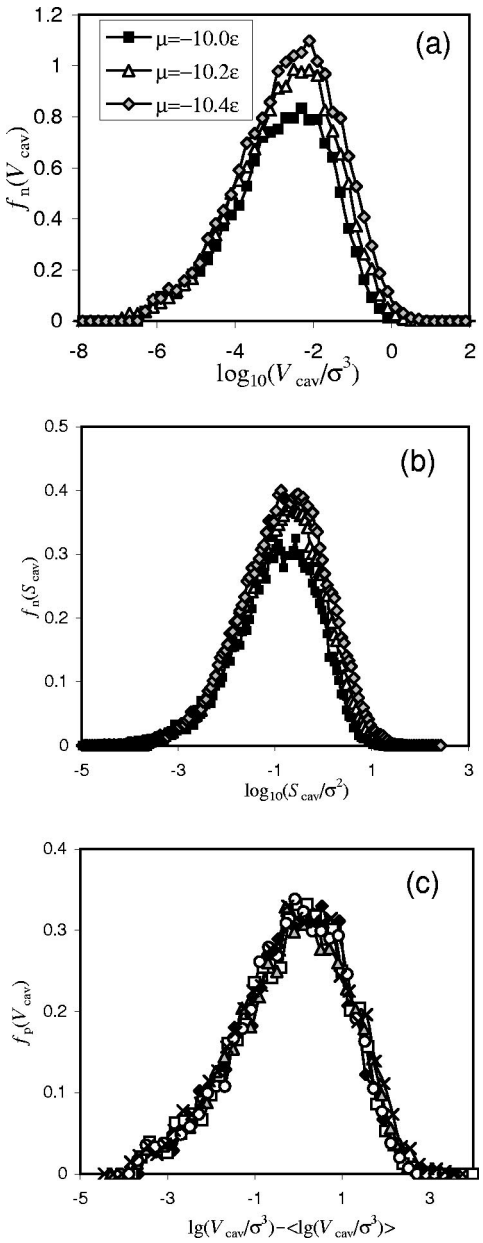

FIG. 6. (a) Number distributions of cavity volumes for three different liquid states on the stable and metastable parts of the desorption isotherm (see text, Sec. III A); (b) the same for cavity surface areas; (c) probability distribution of cavity volumes for seven different liquid states on the desorption isotherm.

III. RESULTS AND DISCUSSION

A. Self-similarity of cavity distributions

The total void volume, the number of cavities, and the distributions of cavity volumes and surface areas were calculated in 11 liquidlike states on the desorption branch of the isotherm. The number of cavities detected and the total void volume in the system increase monotonically as the chemical potential decreases, and with it the fluid density (Fig. 5). No qualitative changes were observed at the equilibrium transition $\mu=\mu_e$. Also, there seems to be no qualitative difference in the cavity volume and surface area distributions between the stable ($\mu_e<\mu<\mu_0$) and metastable states ($\mu_{sl}<\mu<\mu_e$). Figures 6(a) and 6(b) show number distributions of cavity volumes and surface areas [$f_n(V_{cav})$ and $f_n(S_{cav})$, respectively] for three different values of chemical potential on the stable and methastable parts of the desorption branch. The number distributions are not normalized; $f_n(V_{cav})dV_{cav}$ [$f_n(S_{cav})dS_{cav}$] gives the number of cavities with volumes [surface areas] ranging from V_{cav} to $V_{cav}+dV$ [from S_{cav} to $S_{cav}+dS$]. All number distributions are close in shape to the log-normal distribution and shift gradually to larger volumes and surface areas upon decreasing the chemical potential and density [Figs. 6(a) and 6(b)]. Shifting the number distributions by the mean logarithm of the cavity volume and dividing by the average number of cavities in each system, we obtain normalized probability distributions of cavity volumes $f_p(V_{cav})$, shown in Fig. 6(c). The number

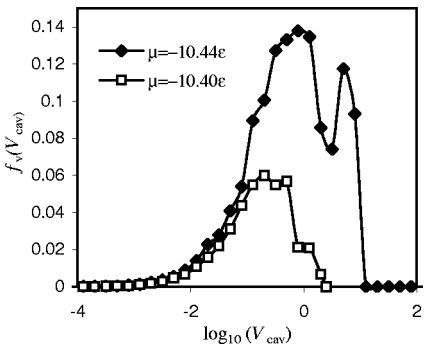

FIG. 7. Cavity volume distributions for $\mu=-10.4\epsilon$ and $\mu=-10.44\epsilon$, close to the spontaneous capillary evaporation transition.

distributions of cavity volumes are essentially similar for all states along the liquid branch and can be approximated by the Gaussian function $f_p(V_{cav})=(2/\pi w^2)^{1/2}\exp[-2\ln(V_{cav}^2/w^2)]$ with the dispersion w close to 2.07.

This result is different from recent observations of Shen and Debenedetti [37], who obtained a bimodal distribution of cavity volumes in superheated bulk liquids with one peak representing the interstitial cavities, which were essentially similar in the stable and metastable states, and the other one corresponding to larger cavities. These larger cavities (ca. $100\sigma^3$ in volume at the top of the free energy maximum at 8.2% superheating) tended to appear as the system overcame the free energy barrier to nucleation. In our simulations of a confined fluid voids of this size were not observed.

B. Appearance of large cavities in the vicinity of the spinodal transition

To reveal relatively large cavities, which might represent nuclei of the vapor phase in the confined liquid, we have plotted the distribution of the void volume contributed by the cavities of certain size to the total void space in the system (Fig. 7). This cavity volume distribution function is related to the number distribution function shown in Fig. 6(a): $f_v(V_{cav})=V_{cav}f_n(V_{cav})$. For the stable and metastable liquid-like states the volume distribution is unimodal. However, as the system approaches the spinodal point $\mu\to\mu_{sl}$, a second maximum appears. The second maximum corresponds to cavities with volumes up to several σ^3. These cavities are much larger than the average cavities yet much smaller than those observed in bulk metastable systems.

C. Pseudocritical behavior at the spinodal point

In a bulk system, density fluctuations (which are proportional to isothermal compressibility) increase in the metastable region. Such fluctuations are predicted to diverge at the spinodal in the limit of systems with infinitely long-range attractions. This mean-field behavior is referred to as pseudocritical [24]. We have examined fluctuations of the cavity volume. The dependence of the mean square volume deviation on the chemical potential is presented in Fig. 8(a). It is clear that the fluctuations of the cavity volume appear to diverge as the spinodal point is approached. In the confined system considered here we cannot expect to observe a true divergence since the correlation length is limited by the pore size. Neglecting finite size effects, we have estimated the

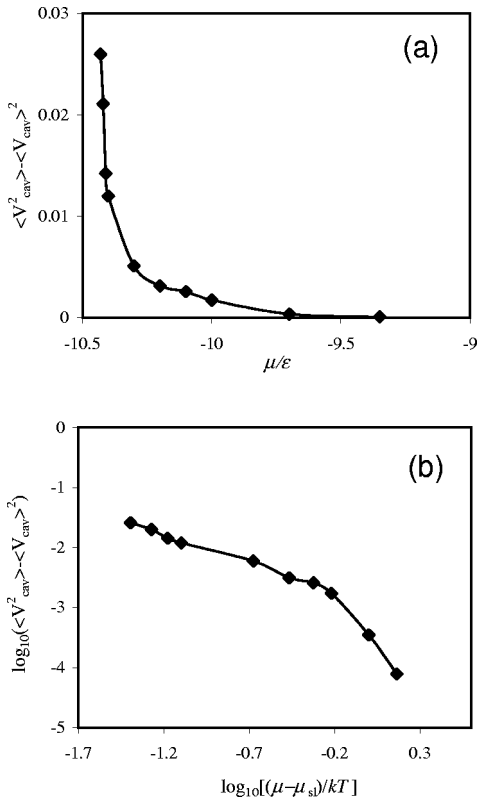

FIG. 8. (a) Dependence of the mean square deviation of the volume of individual cavities from the average on the chemical potential. (b) The same in double-log scale. Line shows the fit to Eq. (1).

spinodal point assuming that dependence of the fluctuation of the cavity volume has the form

$$\log_{10}(\langle V_{cav}^2\rangle-\langle V_{cav}\rangle^2)=-\gamma_c\log_{10}\left(\frac{\mu-\mu_{sl}}{kT}\right)+b, \quad (1)$$

where μ_{sl}, γ_c, and b were treated as adjustable parameters. Figure 8(b) shows that the correlation (1) is satisfied with reasonable accuracy. For the chemical potential corresponding to the desorption spinodal point at a given temperature, we have obtained $\mu_{sl}=-10.45\epsilon$, which almost coincides with the chemical potential $\mu=-10.44\epsilon$ at which spontaneous capillary evaporation has been observed in GCMC simulations. Estimation of the parameter γ_c yielded the value $\gamma_c\approx 0.93$. Thus, at the limit of stability, the cavity volume fluctuations are found to diverge as $(\langle V_{cav}^2\rangle-\langle V_{cav}\rangle^2)\propto[(\mu-\mu_{sl})/kT]^{-\gamma_c}$ with the exponent $\gamma_c\approx 0.93$. This exponent can be referred to as the cavity pseudocritical exponent, analogous to the other pseudocritical exponents characterizing divergence of the thermodynamic quantities at the mean-field spinodal. The cavity pseudocritical exponent is expected to be related to the pseudocritical exponent characterizing divergence of compressibility at the limit of thermodynamic stability, $\mu\to\mu_{sl}$.

D. Surface-to-volume scaling relation for cavities

The shape of the cavities in a confined system is of special interest. Classical nucleation theory assumes a spherical

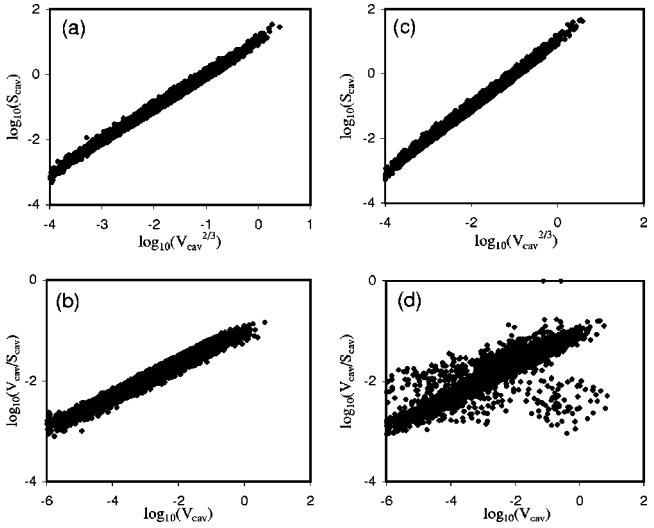

FIG. 9. Dependence of the cavity surface area on the cavity volume at $\mu=-10.40\epsilon$ (*a*,*b*) and at $\mu=-10.44\epsilon$ (*c*,*d*). Only cavities larger than $10^{-6}\sigma^3$ are shown.

shape for the nucleus. However, a recent study of liquid-vapor nucleation in a bulk fluid showed ramified nonspherical cavities [37]. As density decreases, these cavities coalesce and form a large system-spanning cavity, growing as the free energy barrier is overcome. In our study of a fluid confined in a pore of 10 molecular diameters in width, we observed mostly relatively small interstitial cavities. The shape of cavities can be analyzed by comparing their volumes and surface areas. For nonfractal three-dimensional objects, the surface area scales with the volume as $S_{\mathrm{cav}}=gV_{\mathrm{cav}}^{2/3}$. The shape factor g reflects the surface-to-volume ratio for an object of unit volume; for spheres $g=4.83$, for cubic cavities $g=6.0$, for tetrahedra $g=7.20$. For mass fractals such as ramified aggregates, the surface area and volume are expected to be proportional, $S_{\mathrm{cav}}\propto V_{\mathrm{cav}}$, or $S_{\mathrm{cav}}/V_{\mathrm{cav}}\approx$const. In general, the surface-to-volume scaling implies a power law dependence:

$$S_{\mathrm{cav}}=gV_{\mathrm{cav}}^{2a/3} \text{ or } \log_{10}(S_{\mathrm{cav}})=(2a/3)\log_{10}(V_{\mathrm{cav}})+\log_{10}g. \tag{2}$$

The parameter a equals 1 for three-dimensional objects and $\frac{3}{2}$ for mass fractals, while intermediate values are characteristic for surface fractals. In order to check the surface-to-volume scaling, we plotted the relation between the cavity surface area and volume in double logarithmic coordinates in two forms: S_{cav} versus $V_{\mathrm{cav}}^{2/3}$ [Figs. 9(a) and 9(c)] and $V_{\mathrm{cav}}/S_{\mathrm{cav}}$ versus V_{cav} [Figs. 9(b) and 9(d)]. As a typical example, in Figs. 9(a) and 9(b) we present data collected in a metastable state at $\mu=-10.40\epsilon$. The slope of the plot is close to 1 in Fig. 9(a) and to $\frac{1}{3}$ in Fig. 9(b). This regression holds over more than six decades of cavity surface area with a correlation coefficient of 0.995. Similar scaling was found for all liquidlike states on the desorption branch, independent of the chemical potential of the fluid. This shows that the shape of cavities of different sizes is self-similar; cavities are three-dimensional objects and do not display fractal properties. The cavity shape factor g varied from 8.32 to 9.55 depending on the chemical potential. That is, the surface-to-volume ratio for the interstitial cavities, one of which is shown in Fig. 4, is higher than that for tetrahedra.

In Figs. 9(c) and 9(d) we present data collected in the immediate vicinity of the spinodal ($\mu_{sf}=-10.44\epsilon$). In the coordinates S_{cav} versus $V_{\mathrm{cav}}^{2/3}$ [Fig. 9(c)], we observe behavior as in other liquidlike states, which implies that the cavities on average obey three-dimensional (3D) scaling with a linear relationship between their surface area and volume to the power $\frac{2}{3}$. However, in the representation $V_{\mathrm{cav}}/S_{\mathrm{cav}}$ versus V_{cav} [Fig. 9(d)] another type of cavities is revealed. While the vast majority of points lie along the line with slope $\frac{1}{3}$, a relatively small group of cavities forms a cloud of points that deviate from 3D scaling. This group includes the relatively large cavities revealed in Fig. 7. Their surface area is substantially larger (by about one order of magnitude) than the surface area of most of the cavities of the same volume. These cavities are probably considerably more ramified. The statistics is insufficient to draw definitive conclusions regarding their geometry. Based on the plot in Fig. 9(d) we can assume that for the ramified cavities the surface area is roughly proportional to the volume. This points toward a fractal-like shape of the ramified cavities, which appear in the vicinity of the spinodal transition. Further studies are required to confirm whether the ramified cavities are similar to fragments of a spanning percolation cluster.

IV. CONCLUSIONS

Phase transitions in confined fluids, such as capillary condensation and desorption, are characterized by equilibrium stable and metastable states that give rise to the experimentally observable hysteresis phenomena and spinodal transitions. Confined fluid behavior in the vicinity of the spinodal point (the limit of thermodynamic stability) has been investigated by means of GCMC simulations of LJ fluid sorption in nanopores and subsequent Voronoi-Delaunay tessellation analysis of the statistical geometry of intermolecular cavities. We have shown that the cavity size distributions in liquidlike states, characterized by different densities, can be approximated by a universal log-normal distribution function about the mean void volume, which increases as the density decreases. The surface-to-volume relation for individual cavities fulfills the three-dimensional scaling $S_{\mathrm{cav}}=gV_{\mathrm{cav}}^{2/3}$ over six orders of cavity volume. In the immediate vicinity of the spinodal point, as the chemical potential μ approaches the stability limit μ_{sl}, large cavities are formed, which are ramified, with a fractal-like surface-to-volume relation $S_{\mathrm{cav}}\propto V_{\mathrm{cav}}$. Better statistics is needed to check whether or not these ramified cavities are similar to fragments of a spanning percolation cluster. As the system approaches the stability limit $\mu\rightarrow\mu_{sl}$, the cavity volume fluctuations are found to diverge as $(\langle V_{\mathrm{cav}}^2\rangle-\langle V_{\mathrm{cav}}\rangle^2)\propto[(\mu-\mu_{sl})/kT]^{-\gamma_c}$ with the exponent $\gamma_c\approx0.93$. This exponent can be referred to as the cavity pseudocritical exponent in analogy to the other pseudocritical exponents introduced to characterize the divergence of thermodynamic quantities at the spinodal.

ACKNOWLEDGMENTS

The authors gratefully acknowledge helpful discussions with T. Truskett and V. Shen on the application of the tessellation algorithm to confined systems. Work has been supported in part by the TRI/Princeton exploratory research program, the U.S. Environmental Protection Agency (Grant No. R825959-010), and the U.S. Department of Energy, Division of Chemical Sciences, Office of Basic Energy Sciences (Grant No. DE-FG02-87ER13714).

[1] D. H. Everett, in *The Solid-Gas Interface*, edited by E. A. Flood (Marcel Dekker, New York, 1967), Vol. 2, p. 1055.
[2] L. I. Kheifetz and A. V. Neimark, *Multiphase Processes in Porous Media* (Khimiia, Moscow, 1982).
[3] F. Rouquerol, J. Rouquerol, and K. S. V. Sing, *Adsorption by Powders and Porous Solids: Principles, Methodology and Applications* (Academic, San Diego, 1999).
[4] P. I. Ravikovitch, S. C. O'Domhnaill, A. V. Neimark, F. Schuth, and K. K. Unger, Langmuir **11**, 4765 (1995).
[5] A. V. Neimark, P. I. Ravikovitch, M. Grun, F. Schuth, and K. K. Unger, J. Colloid Interface Sci. **207**, 159 (1998).
[6] P. Tarazona, U. Marconi, and R. Evans, Mol. Phys. **60**, 573 (1987).
[7] Sh. Jiang, S. L. Rhykkerd, and K. E. Gubbins, Mol. Phys. **79**, 373 (1993).
[8] W. A. Steele and M. Bojan, Adv. Colloid Interface Sci. **76–77**, 153 (1998).
[9] A. de Keizer, T. Michalski, and G. H. Findenegg, Pure Appl. Chem. **63**, 1495 (1991).
[10] P. I. Ravikovitch, D. Wei, W. T. Chueh, G. L. Haller, and A. V. Neimark, J. Phys. Chem. B **101**, 3671 (1997); P. I. Ravikovitch, G. L. Haller, and A. V. Neimark, Adv. Colloid Interface Sci. **76–77**, 203 (1998).
[11] E. N. Brodskaya and E. M. Piotrovskaya, Langmuir **10**, 1837 (1994).
[12] A. M. Vishnkakov, E. M. Piotrovskaya, and E. N. Brodskaya, Adsorption **4**, 207 (1998).
[13] L. D. Gelb and K. E. Gubbins, Langmuir **15**, 305 (1999).
[14] P. Röcken and P. Tarazona, J. Chem. Phys. **105**, 2034 (1996).
[15] W. Gac, A. Patrikeev, and S. Sokolovsky, Surf. Sci. **306**, 434 (1994).
[16] A. V. Neimark and P. I. Ravikovitch, in *Microscopic Simulation of Interfacial Phenomena in Solids and Liquids*, edited by S. R. Phillpot, P. D. Bristowe, D. G. Stroud, and J. R. Smith, MRS Symposium Proceedings No. 492 (Materials Research Society, Pittsburgh, 1998) pp. 27–33; A. V. Neimark and P. I. Ravikovitch, Stud. Surf. Sci. Catal. (to be published).
[17] A. V. Neimark, P. I. Ravikovitch, and A. Vishnkakov, Phys. Rev. E (to be published).
[18] R. J. Speedy, J. Chem. Soc., Faraday Trans. 2 **76**, 693 (1980).
[19] R. J. Speedy and H. Reiss, Mol. Phys. **72**, 999 (1991).
[20] D. S. Corti and P. G. Debenedetti, Chem. Eng. Sci. **49**, 2717 (1994).
[21] L. Boltzmann, *Lectures on Gas Theory* (University of California Press, Berkeley, 1964).
[22] R. J. Speedy and H. Reiss, Mol. Phys. **72**, 1015 (1991).
[23] D. S. Corti and P. G. Debenedetti, I&EC Res. **34**, 3573 (1995).
[24] A. Compagner, Physica (Amsterdam) **72**, 115 (1974).
[25] R. J. Speedy, J. Phys. Chem. **86**, 982 (1982).
[26] R. J. Speedy, J. Phys. Chem. **86**, 3002 (1982).
[27] S. Sastry, D. S. Corti, P. Debenedetti, and F. H. Stillinger, Phys. Rev. E **56**, 5524 (1997).
[28] S. Sastry, P. G. Debenedetti, and F. H. Stillinger, Phys. Rev. E **56**, 5533 (1997).
[29] S. Sastry, T. Truskett, P. G. Debenedetti, S. Torquato, and F. H. Stillinger, Mol. Phys. **95**, 289 (1998).
[30] J. K. Johnson, J. A. Zollweg, and K. E. Gubbins, Mol. Phys. **78**, 591 (1992).
[31] W. A. Steele, *The Interactions of Gases with Solid Surfaces* (Pergamon, Oxford, 1974).
[32] B. K. Peterson and K. E. Gubbins, Mol. Phys. **62**, 215 (1987).
[33] Y. Hansawa, K. Kaneko, R. W. Pekala, and M. S. Dresselhaus, Langmuir **12**, 6167 (1996).
[34] K. Kaneko, C. Ichii, H. Kanoh, Y. Hanzawa, N. Setoyama, and T. Susuki, Adv. Colloid Interface Sci. **76-77**, 295 (1998).
[35] L. D. Landau and E. M. Lifshitz, *Statistical Physics*, 3rd ed. (Pergamon, London, 1980).
[36] M. Tanemura, T. Ogawa, and N. Ogita, J. Comput. Phys. **51**, 191 (1983).
[37] V. K. Shen and P. G. Debenedetti, J. Chem. Phys. **111**, 3581 (1999).